Elastic wavefield imaging with scalar and vector potentials

Jia Yan* and Paul Sava, Center for Wave Phenomena, Colorado School of Mines

SUMMARY

We demonstrate reverse-time imaging using multicomponent elastic wavefields. The elastic data are used as boundary conditions for a numeric solution to the elastic wave-equation solved using a staggered-grid finite-difference implementation. P and S components are not separated from recorded data, but are extrapolated together as part of a vector wavefield. A straightforward extension to the cross-correlation imaging condition used for imaging scalar wavefields leads to images hard to interpret, since P and S wavefield components are mixed on the vertical and horizontal projections of displacement fields. We use an alternative imaging condition based on elastic potentials, which reduces cross-talk and leads to images that are easier to interpret, since reflections of different wave modes are separated from one-another.

INTRODUCTION

Multicomponent elastic data are commonly recorded in land or marine (ocean-bottom) seismic experiments. Vector elastic wavefields are not usually processed by specifically designed imaging procedures, but they are processed by extensions of techniques used for scalar wavefields. Thus, seismic data processing does not take full advantage of the information contained by elastic wavefields, e.g. for illumination of complex geology, amplitude preserving imaging, estimation of model parameters, etc.

There are two potential approaches to imaging elastic seismic wavefields.

- The first option is to separate P and S modes on the acquisition surface from the recorded elastic wavefields. This procedure involves either approximations about the propagation path and direction of polarization of the recorded data, or it involves reconstruction of the seismic wavefields in the vicinity of the acquisition surface by a numerical solution of the elastic wave-equation, followed by wavefield decomposition in P and S potentials using div ($\nabla \cdot$) and curl ($\nabla \times$) operators (Etgen, 1988; Zhe and Greenhalgh, 1997).

  An alternative data decomposition in P and S potentials is to reconstructed wavefields in the subsurface using the elastic wave-equation, then decompose the wavefields in P and S potential and finally forward extrapolate the separated wavefields back to the surface using the acoustic wave-equation with the appropriate propagation velocity for the P or S wave modes (Sun et al., 2006). Once data are decomposed in P and S potentials, imaging can be done using conventional procedures employed for scalar wavefields for the separated P and S modes.

- The second option is to extrapolate wavefields in the subsurface using a numeric solution to the elastic wave-equation and then apply an imaging condition that extracts reflectivity information from the source and receiver wavefields. In case extrapolation is implemented by finite-difference methods (Chang and McMechan, 1986, 1994), this procedure is known as elastic reverse time migration, and is conceptually similar to acoustic reverse-time migration (Baysal et al., 1985), which is more frequently used in seismic imaging.

Different imaging conditions have been proposed for extracting reflectivity information from elastic wavefields. One possibility is the exitation-time imaging condition proposed by Chang and McMechan (1986). This imaging condition extracts from extrapolated wavefields reflectivity information at times computed by ray tracing from the source. This approach represents a special case of a more general type of imaging condition involving time cross-correlations of source and receiver wavefields at every location in the image.

For vector elastic wavefields, the cross-correlation imaging condition has to be implemented on combinations of components separated from the displacement field. The problem with this type of imaging condition is that the source and receiver wavefields contain a mix of P and S wave modes which hampers interpretation of migrated images. An alternative to this type of imaging is to perform wavefield separation in P and S potentials *after* wavefield reconstruction in the imaging volume, but prior to the imaging condition and then cross-correlate pure P and S modes from the source and receiver wavefields, as suggested by Dellinger and Etgen (1990).

We investigate this form of imaging using potentials decomposition after extrapolation and demonstrate that it can, indeed, be used to construct images corresponding to combinations of pure P and S modes. The images obtained by this procedure suffer from less cross-talk between wave modes that are not separated on vertical and horizontal components of the reconstructed wavefields. However, even images obtained by this procedure are not free from artifacts, since back-propagation of vector fields from the receivers triggers sources of artificial wave modes that are not part of the recorded wavefields.

IMAGING CONDITION

Assuming single scattering in the Earth (Born approximation), a conventional imaging procedure consists of two components: wavefield extrapolation and imaging. Wavefield extrapolation is used to reconstruct in the imaging volume the seismic wavefield using the recorded data on the acquisition surface as boundary condition, and imaging is used to extract reflectivity information from the extrapolated source and receiver wavefields.

Scalar wavefield imaging

Assuming scalar recorded data, wavefield extrapolation using a scalar wave-equation reconstructs scalar source and receiver wavefields at every location in the subsurface, $u_s(x,z,t)$ and $u_r(x,z,t)$. We can use one-way or two-way wavefield extrapolation implemeted by differential or integral methods. Using the scalar extrapolated wavefields u_s and u_r, a conventional imaging condition (Claerbout, 1985) can be implemented as cross-correlation at zero-lag time:

$$I(x,z) = \int u_s(x,z,t) u_r(x,z,t) dt . \qquad (1)$$

$I(x,z)$ denotes a scalar image obtained from scalar wavefields $u_s(x,z,t)$ and $u_r(x,z,t)$. Equation (1) generalizes trivially to 3D.

Displacement imaging condition

Assuming vector data, wavefield extrapolation using a vector wave-equation reconstructs source and receiver wavefields at every location in the subsurface, $\mathbf{u}_s(x,z)$ and $\mathbf{u}_r(x,z)$. Here, $\mathbf{u}_s$ and $\mathbf{u}_r$ represent the source and receiver displacement fields recorded by multicomponent geophones. Using the vector extrapolated wavefields $\mathbf{u}_s = \{u_{sx}, u_{sz}\}$ and $\mathbf{u}_r = \{u_{rx}, u_{rz}\}$, we can formulate an imaging condition as a straightforward extension of (1). In this case, we can cross-correlate all combinations of components of the source and receiver

Elastic wavefield imaging

wavefields. Such an imaging condition can be formulated mathematically as:

$$I_{zz}(x,z) = \int u_{sz}(x,z,t)\,u_{rz}(x,z,t)\,dt\,, \tag{2}$$

$$I_{zx}(x,z) = \int u_{sz}(x,z,t)\,u_{rx}(x,z,t)\,dt\,, \tag{3}$$

$$I_{xz}(x,z) = \int u_{sx}(x,z,t)\,u_{rz}(x,z,t)\,dt\,, \tag{4}$$

$$I_{xx}(x,z) = \int u_{sx}(x,z,t)\,u_{rx}(x,z,t)\,dt\,. \tag{5}$$

$I_{zz}(x,z)$ represents the image component produced by cross-correlation of the z components of the source and receiver wavefields, $I_{zx}(x,z)$ represents the image component produced by cross-correlation of the z component of the source wavefield with the x component of the receiver wavefield, etc. Equations (2)-(5) generalize trivially to 3D.

The main drawback of applying this type of imaging condition is that the wavefields used for imaging contain a combination of P and S wave modes. Those wavefields interfere with one-another in the imaging condition, since the P and S components are not separated in the extrapolated wavefields. The cross-talk between various components of the wavefield creates artifacts and makes it difficult to interpret the images in terms of pure modes, e.g. PP or PS reflections. This situation is similar to the case of imaging with acoustic data contaminated by multiples or other types of coherent noise.
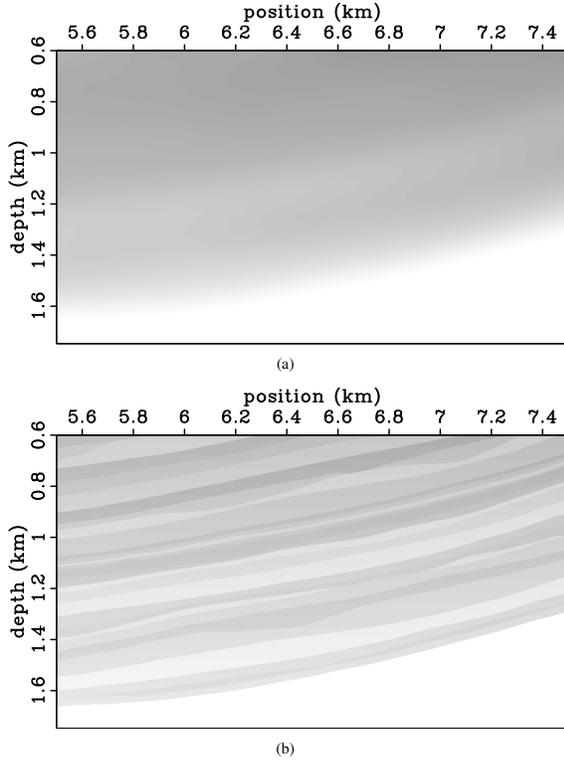

(a)

(b)

Figure 1: P- and S-wave velocity models (a) and density model (b) used for isotropic elastic wavefield modeling.

For illustration, consider the images obtained for the model depicted in Figures 1(a)-1(b). Figure 1(a) depicts the P-wave velocity (smooth function between $1.6 - 3.2$ km/s), and figure 1(b) shows the density (variable between $1 - 2$ g/cm^3). The S-wave velocity is a scaled version of the P-wave velocity with $v_p/v_s = 2$. Data are modeled and

migrated in the smooth velocity background to avoid back-scattering; the modeling density is shown in figure 1(b), and the migration density is a smooth version of it.

Elastic data, figures 2(a)-2(b), are simulated using a space-time staggered-grid finite-difference solution to the isotropic elastic wave-equation (Virieux, 1984, 1986; Mora, 1987, 1988). We model data by simulating a source located at position $x = 7$ km and $z = 0.55$ km. Since we are using an explosive source, the simulated wavefield is represented by P-wave incident energy and the receiver wavefield is represented by a combination of P- and S-wave reflected energy. The data contain a mixture of P and S modes, as can be seen by comparing the displacement field components in figures 2(a)-2(b) with the separated P and S components in figures 2(c)-2(d).

If we image data shown in figures 2(a)-2(b) using the imaging condition (2)-(5), we obtain the images depicted in figures 3(a)-3(d). The imaging condition does not separate P and S waves reflectivity, therefore the various panels contain energy from both wave modes.

Potentials imaging condition

An alternative to the elastic imaging condition (2)-(5) is to separate the extrapolated wavefields in P and S potentials after extrapolation and image using cross-correlations of vector and scalar potentials (Dellinger and Etgen, 1990).

Separation of scalar and vector potentials can be achieved by Helmholtz decomposition, which is applicable to any vector field **u**:

$$\mathbf{u} = \nabla\theta + \nabla \times \psi\,. \tag{6}$$

For isotropic elastic wavefields, equation (6) is not used directly in practice, but the scalar and vector components are obtained indirectly by the application of the $\nabla \cdot$ and $\nabla \times$ operators to the extrapolated elastic wavefields **u**:

$$\Theta = \nabla \cdot \mathbf{u} = \nabla^2\theta\,, \tag{7}$$

$$\Psi = \nabla \times \mathbf{u} = \nabla \times \nabla \times \psi\,. \tag{8}$$

For isotropic elastic fields, quantities Θ and Ψ describe P and S components, respectively (Aki and Richards, 2002).

Using the separated scalar and vector components, we can formulate an imaging condition that combines various incident and reflected wavefield components. In 2D, the vector potential $\Psi(x,z,t)$ has only one component. The imaging condition for potentials can be formulated mathematically as:

$$I_{PP}(x,z) = \int \Theta_s(x,z,t)\,\Theta_r(x,z,t)\,dt\,, \tag{9}$$

$$I_{PS}(x,z) = \int \Theta_s(x,z,t)\,\Psi_r(x,z,t)\,dt\,, \tag{10}$$

$$I_{SP}(x,z) = \int \Psi_s(x,z,t)\,\Theta_r(x,z,t)\,dt\,, \tag{11}$$

$$I_{SS}(x,z) = \int \Psi_s(x,z,t)\,\Psi_r(x,z,t)\,dt\,, \tag{12}$$

where $\Theta_s(x,z,t)$ and $\Theta_r(x,z,t)$ represent source and receiver P-wave components, and $\Psi_s(x,z,t)$ and $\Psi_r(x,z,t)$ represent source and receiver S-wave components. The formed images correspond to various combinations of incident P or S and reflected P or S waves.

For illustration, consider the images obtained for imaging condition **??-??** applied to the data used for the preceding example. Given the explosive source used in our simulation, the source wavefield contains mostly P-wave energy, while the receiver wavefield contains P- and S-wave energy. Helmholtz decomposition after extrapolation but prior
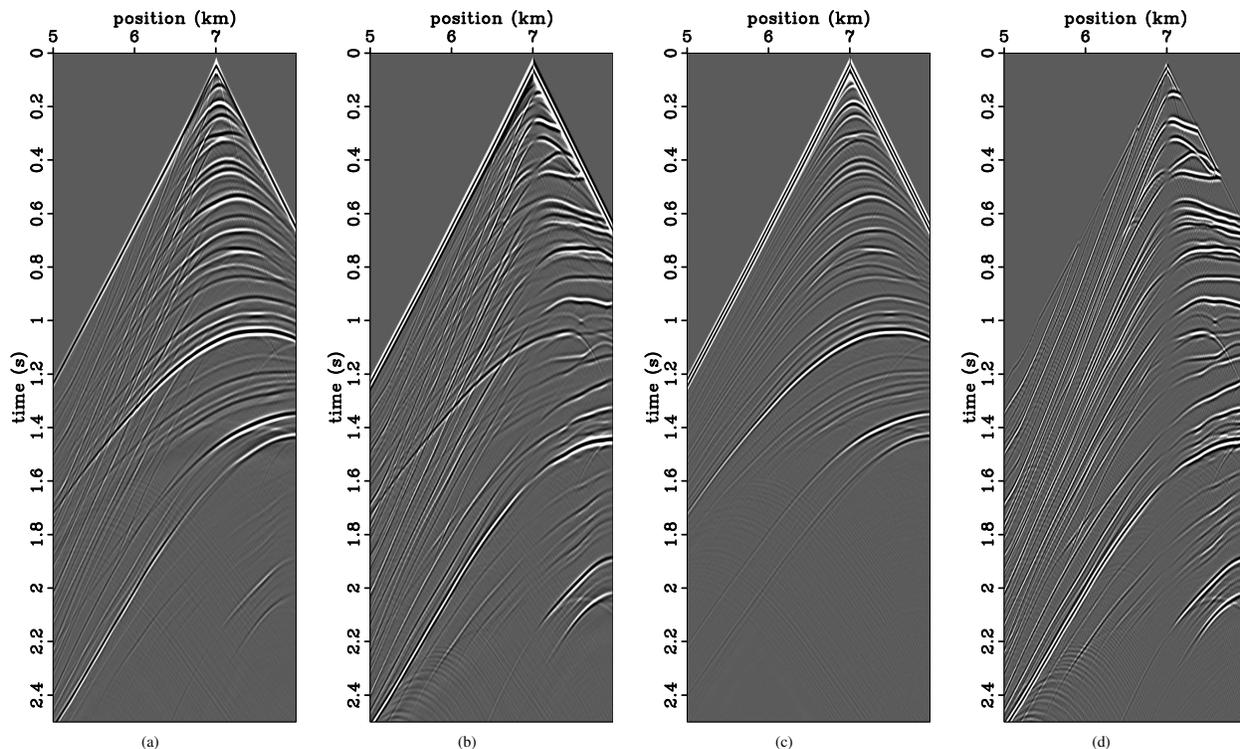
Elastic wavefield imaging

Figure 2: Elastic data simulated in model 1(a)-1(b): vertical component (a), horizontal component (b), scalar potential (c) and vector potential (d) of the elastic wavefield. Both vertical and horizontal components, panels (a) and (b), contain a mix of P and S modes, as seen by comparison with panels (c) and (d).

to imaging isolates P and S wavefield components. Therefore, migration produces images of reflectivity corresponding to PP and PS reflections, figures 4(a)-4(b), but not reflectivity corresponding to SP or SS reflections, figures 4(c)-4(d). As expected, the illumination regions are different between PP and PS images, due to different illumination angles of the two propagation modes for the given acquisition geometry. The PS image, figure 4(b), also shows the usual polarity reversal for positive and negative angles of incidence measured relative to the reflector normal.

DISCUSSION

One drawback of reverse-time migration using elastic wavefields is that back-propagating with recorded displacement data as boundary conditions generates spurious events that do not exist in the original wavefield. For example, data corresponding to P-wave or S-wave reflections injected in the model as boundary displacement sources generate both P and S propagating modes. Those artificial events in the receiver wavefield interfere with events in the source wavefield to generate artifacts in the images. This phenomenon is independent of the complexity of the model or of the proximity of free surface.

An example corresponding to artifacts caused by artificial P waves generated by back-propagating S waves in the receiver wavefield are visible in figure 4(a) around coordinates $x = 7.25$ km and $z = 0.6$ km. Although not widely reported in the literature, this phenomenon characterizes all elastic reverse-time migration methods, no matter of imaging condition. For example, the same artifacts seen in figures 4(a)-4(b) are also seen in figures 3(a)-3(d), although in this case the artifacts are more confusing, since their origin is harder to discern among the imaged reflections of different wave modes.

CONCLUSIONS

The elastic reverse-time migration imaging condition can be formulated using decomposition of extrapolated wavefields in P and S components. The formed images separate reflections corresponding to forward-propagating P or S modes and backward propagating P or S modes. In contrast, images formed by simple cross-correlation of displacement wavefield components mix contributions from P and S reflections and are harder to interpret. Artifacts caused by back-propagating the recorded data with displacement sources are present in both types of images, although they are easier to distinguish and attenuate on the images constructed with elastic components separated prior to imaging.
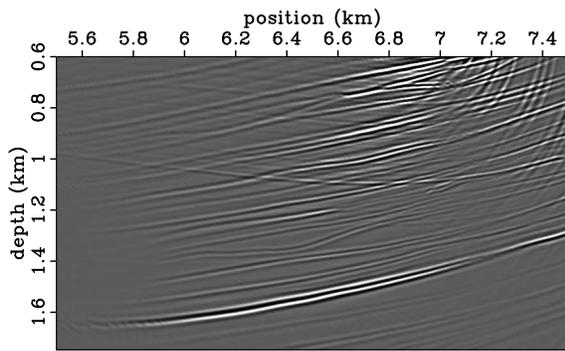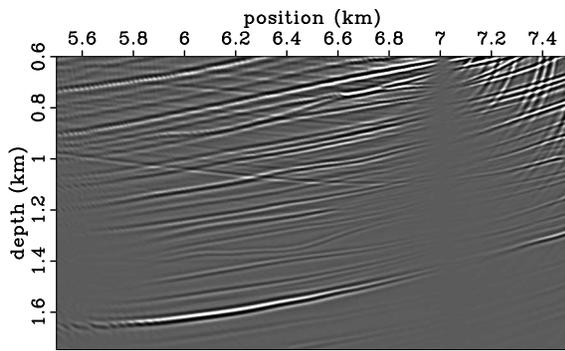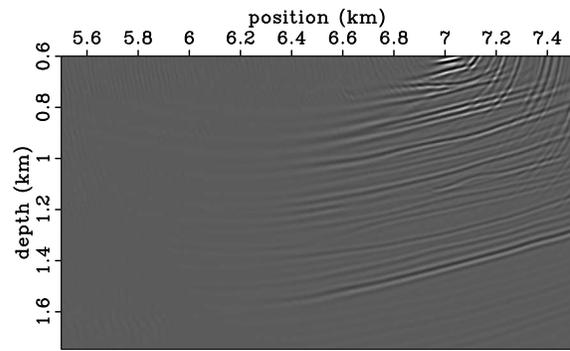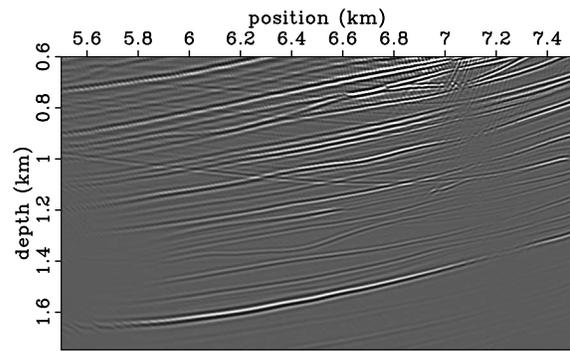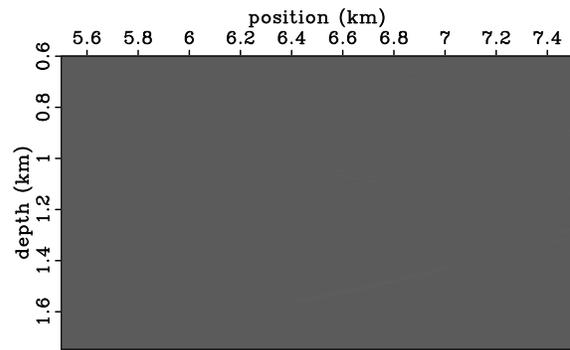
ACKNOWLEDGMENT
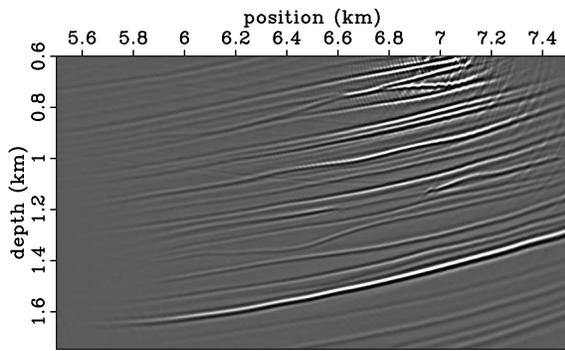
(a)

(b)
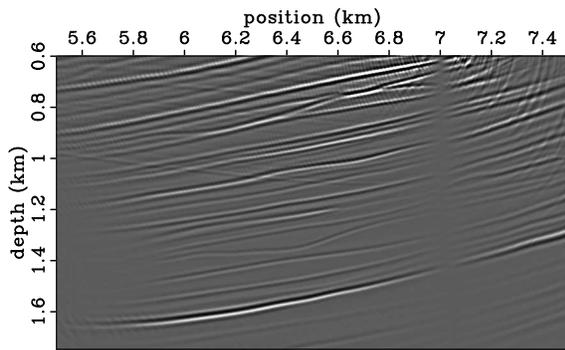
(c)

(d)

Figure 3: Images produced by the application of the displacement imaging condition (2)-(5). The image corresponds to one shot at position $x = 7$ km. Receivers are located at all locations at $z = 0.55$ km.
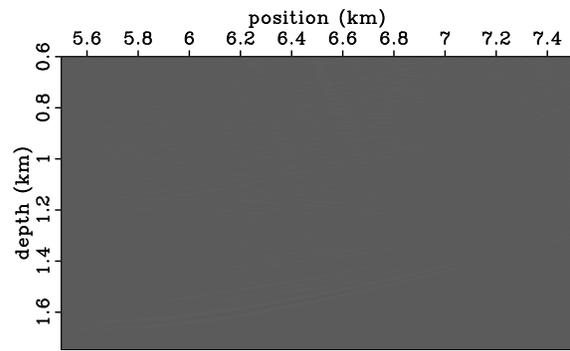
Figure 4: Images produced by the application of the potentials imaging condition (9)-(12). The image corresponds to one shot at position $x = 7$ km. Receivers are located at all locations at $z = 0.55$ km.

Elastic wavefield imaging

REFERENCES

Aki, K. and P. Richards, 2002, Quantitative seismology (second edition): University Science Books.

Baysal, E., D. D. Kosloff, and J. W. C. Sherwood, 1985, Reverse time migration, *in* Gardner, G. H. F., ed., Migration of seismic data, 452–462, Soc. of Expl. Geophys. Reprinted from Geophysics, 48, 1514-1524.

Chang, W. F. and G. A. McMechan, 1986, Reverse-time migration of offset vertical seismic profiling data using the exitation-time imaging condition: Geophysics, **51**, 67–84.

——, 1994, 3-D elastic prestack, reverse-time depth migration: Geophysics, **59**, 597–610.

Claerbout, J. F., 1985, Imaging the Earth's interior: Blackwell Scientific Publications.

Dellinger, J. and J. Etgen, 1990, Wave-field separation in two-dimensional anisotropic media (short note): Geophysics, **55**, 914–919.

Etgen, J. T., 1988, Prestacked migration of P and Sv-waves: 58th Ann. Internat. Mtg, Session:S12.4, Soc. of Expl. Geophys.

Mora, P., 1988, Elastic wave-field inversion of reflection and transmission data: Geophysics, **53**, 750–759.

Mora, P. R., 1987, Nonlinear two-dimensional elastic inversion of multioffset seismic data: Geophysics, **52**, 1211–1228.

Sun, R., G. A. McMechan, C.-S. Lee, J. Chow, and C.-H. Chen, 2006, Prestack scalar reverse-time depth migration of 3d elastic seismic data: Geophysics, **71**, S199–S207.

Virieux, J., 1984, SH-wave propagation in heterogeneous media - Velocity-stress finite-difference method: Geophysics, **49**, 1933–1942.

——, 1986, P-Sv wave propagation in heterogeneous media - Velocity-stress finite-difference method: Geophysics, **51**, 889–901.

Zhe, J. and S. A. Greenhalgh, 1997, Prestack multicomponent migration: Geophysics, **62**, 598–613.